Coaxial Probe Modeling in Waveguides and Cavities

Ji-Fuh Liang, Hsin-Chin Chang, and Kawthar A. Zaki, *Fellow, IEEE*

Abstract—**Modeling, design and sensitivity analysis of probe-excited cavities are presented. The 3 cavities moment method is used to obtain the 2-port scattering matrix of the probe-excited semi-infinite waveguide while a novel equivalent circuit is introduced and used as a circuit model for the scattering matrix. A design procedure for probe-excited input/output cavities in waveguide filters is proposed and a sensitivity analysis is carried out to show the effect of the probe's dimensions on the electrical characteristics of the circuit. Agreement with experimental data is excellent for loosely-coupled probe-excited semi-infinite waveguide problems. An example for a 15 GHz thick iris filter verifies the validity of the proposed design.**

I. Introduction

THE INPUT and output ports of microwave cavity filters are sometimes realized by coaxial probe-excited cavities [1], [2] to avoid using extra coaxial waveguide transitions. The probe-excited waveguide problem has been treated for three decades [3]–[5], but the efforts were mainly focused on calculating the input impedance as a function of waveguide and probe dimensions to design good adaptors. There are no accurate theoretical models in the literature for predicting the 2-port scattering matrix of coaxial probe excited cavities or the loading effects of the probe on the resonant frequencies. There is also no circuit model to describe the behavior of the junction that can be incorporated into the microwave filter design. The traditional method of probe-excited input/output cavity design is experimental. The depth of the probe is determined empirically, usually requires additional tuning screws to fine-tune the resonance frequency [1]. The frequency responses of the filter cannot be accurately predicted before manufacturing and the cut-and-try process is difficult and time-consuming. If the 2-port scattering matrix of the coaxial-waveguide junction is available, improvement in the design of the probe-excited cavity problem is possible, leading to accurate designs of filters which require no tuning. Such designs could be used to realize miniature dielectric filled waveguide filters, suitable for inexpensive mass production techniques.

In Section II, it is shown how the input impedances (or input reflection coefficients) of 3 cavities can be used to set up three linear equations for obtaining the 2-port scattering matrix of a probe-excited semi-infinite waveguide. The moment method (MM) is used to calculate the input impedance of the probe-excited cavity. In Section III, a circuit model consisting of an impedance inverter and two sections of transmission lines is proposed to represent the scattering matrix of the structure; and a new design procedure for the input/output probe excited cavities of waveguide filters is outlined. Effects of dimensional tolerances of the probe and cavity on the electrical performance of the filter are analyzed. Section IV shows examples of calculated and experimental scattering matrices of probe-excited loosely-coupled semi-infinite waveguides. An experimental filter was designed and tested with good agreement between the numerical results and experimental data.

Manuscript received July 10, 1992; revised July 30, 1992.

The authors are with the University of Maryland, Electrical Engineering Department, College Park, MD 20742.

IEEE Log Number 9203689.

II. Determination of Two-Port Scattering Matrix Using 3 Cavities Solution

Consider the problem of determining (by measurement or by numerical calculation) the two-port scattering matrix of the probe-excited waveguide shown in Fig. 1(a) with scattering matrix representation shown in Fig. 1(b). The elements of the scattering matrix S_{11} and S_{21} can be determined by finding the reflected wave (in the coaxial line) and transmitted wave (in the waveguide side) due to an incident wave in the coaxial line. In a similar way, S_{22} and S_{12} can be determined by calculating the reflected wave (in the waveguide) and transmitted wave (in the coaxial line) due to an incident wave in the waveguide. Alternatively, it is possible to extract the 2-port scattering matrix by impressing the incident wave in the coaxial line only. If port 2 in Fig. 1.(b) is terminated by three different known lengths (L_i, $i = 1, 2, 3$) of shorted guides, and the corresponding input reflection coefficients at port 1 $\Gamma_i (i = 1, 2, 3)$ are measured (or computed), then it can be shown that the 2-port scattering matrix elements can be calculated by solving the following matrix equations [6]:

$$\begin{bmatrix} 1 & \Gamma_1\Gamma_{L_1} & \Gamma_{L_1} \\ 1 & \Gamma_2\Gamma_{L_2} & \Gamma_{L_2} \\ 1 & \Gamma_3\Gamma_{L_3} & \Gamma_{L_3} \end{bmatrix} \begin{bmatrix} S_{11} \\ S_{22} \\ S_{12}S_{21} - S_{11}S_{22} \end{bmatrix} = \begin{bmatrix} \Gamma_1 \\ \Gamma_2 \\ \Gamma_3 \end{bmatrix} \quad (1)$$

The reflection coefficients of the shorted guides are $\Gamma_{L_i} = -e^{-j2\beta L_i}$, $i = 1, 2, 3$, where β is the guide propagation constant and L_i are the lengths of the shorted guides. The measurement configuration is shown in Fig. 1(c). For accuracy, the phases of the reflection coefficient of the terminating short-circuited waveguide sections should not have 360° differences at the frequencies of interest. The best condition is that these phases differ by 120° and 240°.

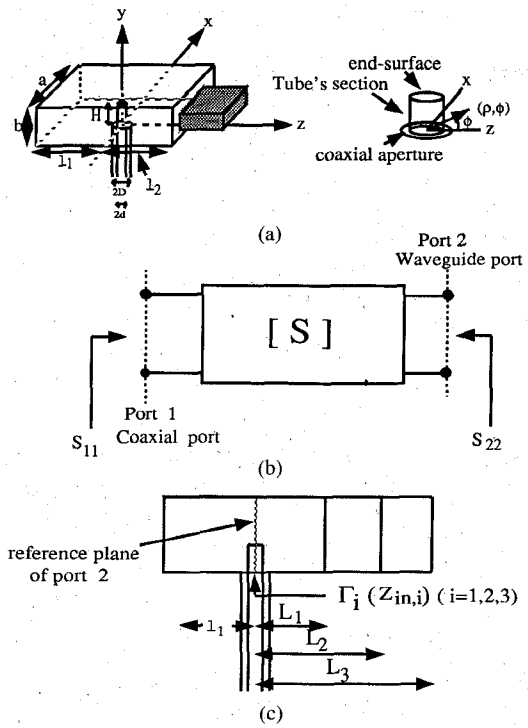

Fig. 1. (a) Coaxial probe-excited semi-infinite waveguide. (b) Scattering matrix representation. (c) Three shorted guides used to extract two port scattering matrix.

Moment Method Solution of Probe-Excited Cavity

To compute the reflection coefficients Γ_i, the moment method is used to calculate the input impedances of the probe-excited cavities of Fig. 1(c). The formulation is similar to the semi-infinite waveguide problem [5] and is briefly summarized here. Assuming that the aperture field is a coaxial TEM mode, then the field at the aperture is a function of the coaxial terminal voltage (V) at the junction. According to the equivalence principle [3], [7], this aperture field can be replaced by an equivalent magnetic current source backed by a perfect electric conductor. This equivalent magnetic current source is given as a function of voltage as

$$\vec{M}_a = \frac{V}{\rho \cdot ln(d/D)} \vec{a}_\phi, \qquad \text{for } d \le \rho \le D \tag{2}$$

where ρ, d and D are defined in Fig. 1(a).

For a thin probe, the effect of the probe's end surface can be neglected, then only y-directed electric current flows on the probe. The Green's function of a y-directed electric current element on the probe and the x- and z-directed magnetic currents on the aperture are derived and must be converted to a fast-convergent series for the cavity in a similar way for the semi-infinite waveguide [3], [5], [8].

The field due to each source is represented as an integral of the product of its source and a Green's function [7]. The total electric fields along the probe axis (i.e., y-direction) in the cavity are the summation of the radiation field due to electric currents on the probe and the

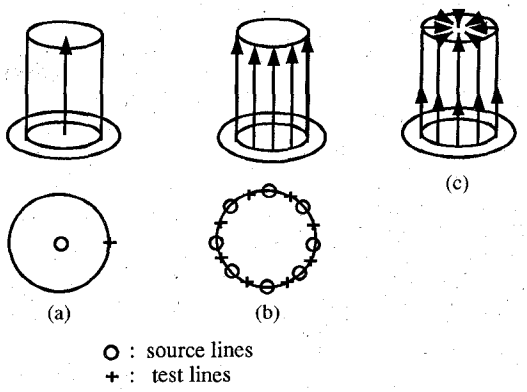

Fig. 2. (a) One-filament axially-concentrated current approximation. (b) Multifilament current approximation. (c) Real current flow on probe.

scattered field due to magnetic currents at the aperture:

$$\vec{E}_{y,\text{total}} = \left(-j\omega + \frac{\partial^2}{j\omega\mu\epsilon\partial y^2}\right) \int_{\text{probe}} G_{A_{yy}} J_y \, ds' - \frac{1}{\epsilon}\left\{\frac{\partial}{\partial z}\int_{\text{aperture}} M_x G_{F_{xx}} \, ds' - \frac{\partial}{\partial x}\int_{\text{aperture}} M_z G_{F_{zz}} \, ds'\right\} \tag{3}$$

where J_y is the electric current on the probe while M_x, M_z are the x- and z-components of the magnetic current at aperture, $G_{A_{yy}}$, $G_{F_{xx}}$, and $G_{F_{zz}}$ are the Green's functions defined in the Appendix. Forcing the tangential electric field on the probe's surface to be zero, the electric current on the probe can be determined by moment method. The input impedance is computed as the ratio of the input terminal voltage at the coaxial aperture divided by the electric current on the probe at the coaxial-waveguide junction, as in [5]. Expressions for the Green's function and its transformation to faster converging series to be used in numerical calculations are shown in the Appendix. The details of the numerical procedure of the moment method can be found in [5] and [9].

The current approximations on the probe used in this paper are shown in Fig. 2.(a) and (b). The 1 filament axially-concentrated current approximation in Fig. 2(a) is widely used in dipole antenna problems, while the multifilament current approximation in Fig. 2(b) is suggested by [5]. Fig. 2(a) and (b) also show the lines where the boundary conditions are enforced. The real current flows on the probe as shown in Fig. 2(c); the current is distributed over all the probe's surface, including the end surface.

For filter applications the probe-excited cavity is usually a loosely-coupled resonator, and the probe's depth H is always much smaller than the operating wavelength. A one term trial function is used to expand the induced probe's current in the y direction. In this paper, the following two functions are used and compared.

$$\sin k_o(y - H) \tag{4}$$

$$\sin \frac{\pi}{2H}(y - H) \tag{5}$$

The first is widely used in dipole antenna problems [10], the 2nd one is the first term of the expansion functions, $\sin n\pi/2H\,(y - H)$ [11], where n is a positive integer.

III. Circuit Representation, Design, and Sensitivity Considerations

Circuit Representation and Design

Once the scattering matrix is obtained from the numerical model, a circuit representation can be made to describe the model behavior as a function of dimensions. For all pole microwave filters, the basic circuit blocks are the impedance (or admittance) inverters and resonators as shown in Fig. 3.(a) [12]. The probe's circuit representation in Fig. 3.(b) is preferred to T- or π-networks as in [12]. The element values in Fig. 3(b) can be derived directly from the junction scattering matrix by imposing the lossless (unitary) and reciprocal conditions. The results are

$$\frac{K_{01}}{\sqrt{Z_c Z_w}} = \sqrt{\frac{1 - |S_{22}|}{1 + |S_{22}|}} \tag{6}$$

$$\phi_i = -\frac{1}{2}\theta_i + \frac{\pi}{2} \qquad i = 1, 2 \tag{7}$$

or

$$\frac{K_{01}}{\sqrt{Z_c Z_w}} = \sqrt{\frac{1 + |S_{22}|}{1 - |S_{22}|}} \tag{8}$$

$$\phi_i = -\frac{1}{2}\theta_i \qquad i = 1, 2 \tag{9}$$

where θ_i is the phase of S_{ii}, Z_c, Z_w are the characteristic impedance of coaxial line and waveguide respectively. It can also be shown that the phase of S_{21} is equal to $(\frac{1}{2}(\theta_1 + \theta_2) - \pi/2 + n\pi)$, where n is an integer. For odd n, (6), (7) should be chosen while (8), (9) should be used for even n. Either set of equations will result in the same absolute values of the insertion loss response of the filter. The value of K_{01} can also be related to the external Q of the input/output cavity [12] as

$$Q_e = \frac{\frac{\pi}{2}}{\left(\frac{K_{01}}{\sqrt{Z_w Z_c}}\right)^2}\left(\frac{\lambda_{go}}{\lambda_o}\right)^2 \tag{10}$$

where λ_{go} is the guide wavelength, λ_o is the free space wavelength.

It is worth noticing that ϕ_2 in Fig. 3(b) (which is related to the phase of S_{22} by (7) or (9)) should be combined with adjacent cavity in the design process. This suggested that the characterization of the port 2 as defined in Fig. 1(b) is preferred for microwave filter design and the choice of the reference plane at the input port is not important. In (6) and (8), $|S_{22}|$ is used rather than $|S_{11}|$ in order to emphasize this. This is also true for other asymmetrical coupling structures. Thus the design parameters needed in the filter design based on the junction characterization are K and ϕ_2 only.

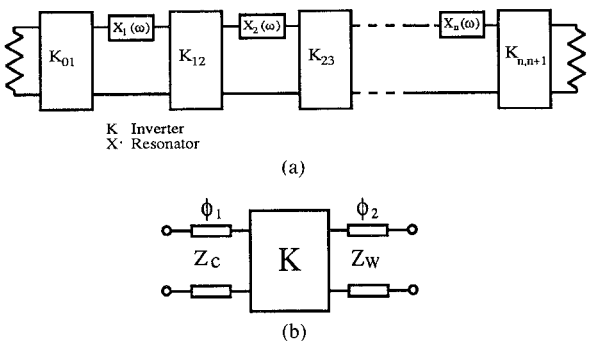

Fig. 3. (a) Microwave filter model as cascade of resonators and inverters. (b) A circuit representation of a lossless, reciprocal junction.

Based on the techniques described above, a new accurate design technique for probe-excited waveguide cavities is proposed as follows:

1. Choose l_1 in Fig. 1(a) at about one quarter wavelength at the resonant frequency.
2. Compute the required magnitude of S_{22}, i.e. $|S_{22}|$, by (6) or (8) for given K or (6), (8) and (10) for given external Q.
3. Optimize the probe depth H to obtain the required $|S_{22}|$ in step 2.
4. Determine l_2' (which is the location of the shorted plane to have the cavity resonate at the desired center frequency) by shifting the phase of S_{22} to 180°. Then take into account the phase offset of the coupling circuit of the next cavity (i.e. reduce the electrical length l_2' by $-\theta/2$, where θ is the phase of the input reflection coefficient of the coupling circuit) to obtain the correct l_2.
5. Compute the filter response by cascading the scattering matrices of the probe-excited cavities sections and the other elements of the filter.

The dispersive nature of the element values in the circuit representation of the probe-excited cavity will contribute some deviation of the response from the ideal. It can be improved by optimizing around the design dimensions obtained from the above procedure. However the other elements of the microwave filter should undergo the same correction procedure.

Sensitivity Considerations

Waveguide cavity filters are more suitable for narrow or moderate bandwidths (a few percent of center frequency). The filter response is very sensitive to the variations of the structure dimensions, especially at high frequencies. The undesired deviations of the filter response from the ideal result from two sources: one is inaccurate component modeling, the other manufacturing errors or tolerances.

The residual reflection coefficient in the passband $\delta\rho$ (defined as the maximum passband reflection coefficient of the perturbed response minus the one without perturbation), due to the small perturbations of the probe's di-

mension ξ is

$$\delta\rho_\xi = S_K^\rho S_\xi^K \delta\xi + S_f^\rho S_\xi^f \delta\xi \tag{11}$$

where ξ is H or d and f is the cavity resonant frequency. The sensitivities S_K^ρ, S_ξ^K, S_f^ρ and S_ξ^f in (11) are defined as

$$S_K^\rho = \frac{\partial\rho}{\partial K/K} = \frac{\partial\rho}{\partial \ln K} \tag{12}$$

$$S_f^\rho = \frac{\partial\rho}{\partial f/f} = \frac{\partial\rho}{\partial \ln f} \tag{13}$$

$$S_\xi^f = \frac{\partial f/f}{\partial\xi} = \frac{\partial \ln f}{\partial\xi} \tag{14}$$

$$S_\xi^K = \frac{\partial K/K}{\partial\xi} = \frac{\partial \ln K}{\partial\xi} \tag{15}$$

The sensitivity of ρ w.r.t. ξ can then be written as

$$S_\xi^\rho = S_K^\rho S_\xi^K + S_f^\rho S_\xi^f \tag{16}$$

The design parameter K is the value of the impedance inverter of the input/output stage in Fig. 3(a), and the phase ϕ_2 affects the resonant frequencies of the input/output resonators. If the computed design parameters K and ϕ_2 have deviations δK and $\delta\phi_2$ from the desired values, the perturbations in passband reflection coefficient can be written as:

$$\delta\rho_K = S_K^\rho \delta \ln K \tag{17}$$

$$\delta\rho_{\phi_2} = S_{\phi_2}^\rho \delta\phi_2 = S_f^\rho \frac{\partial \ln f}{\partial\phi_2}\delta\phi_2 \tag{18}$$

The sensitivity of ρ w.r.t. K has been given in (12) and the sensitivity of ρ w.r.t. ϕ_2 is

$$S_{\phi_2}^\rho = S_f^\rho \frac{\partial \ln f}{\partial\phi_2} = S_f^\rho S_{\phi_2}^f \tag{19}$$

In summary, (16) expresses how the variation of probe dimensions affects the filter passband performance and can be used to determine the tolerance of the dimensions. The required sensitivities are: S_K^ρ, S_f^ρ, S_ξ^K and S_ξ^f. Equations (12) and (19) provide the impact of the model's errors and can be used to determine the accuracies required in the parameter determination.

IV. Results and Discussions

All the sample numerical and measured data discussed below and shown in Figs. 4 to 9 were obtained for a WR62 Waveguide ($a = 0.622''$, $b = 0.311''$) and an SMA coaxial probe (inner diameter: $2d = 0.050''$, outer diameter: $2D = 0.132''$ and characteristic impedance: $Z_c = 50\ \Omega$).

Figs. 4 and 5 show the computed and experimental results of the magnitude and phase of input reflection coefficients of probe-excited semi-infinite waveguide. The computed moment method solutions are obtained and shown for four cases:

1. Using 3 shorted lengths of waveguides (cavities) and 1 filament axially-concentrated probe current, as shown in Fig. 2(a)

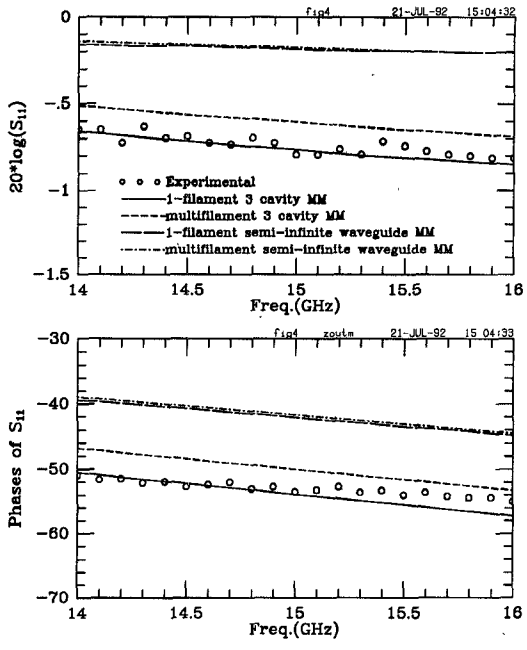

Fig. 4. Numerical and measured S_{11} for a probe-excited semi-infinite waveguide. (Probe depth: $H = 0.051''$).

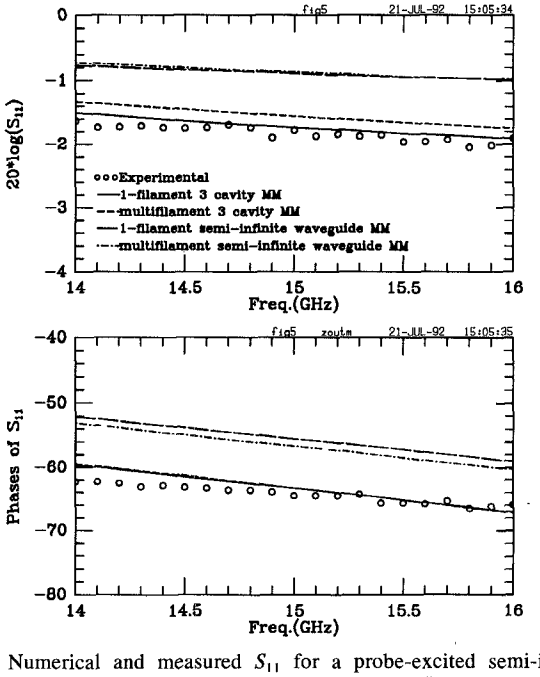

Fig. 5. Numerical and measured S_{11} for a probe-excited semi-infinite waveguide. (Probe depth: $H = 0.078''$).

2. Using 3 shorted lengths of waveguides (cavities) and multifilament probe current, as shown in Fig. 2(b)
3. Using semi-infinite waveguide and 1 filament axially-concentrated probe current
4. Using semi-infinite waveguide and multifilament probe current

A single expansion function is used for the probe current in the probe's direction in the case of cavity, i.e., $\sin k_o(y - H)$. For the semi-infinite waveguide cases, two expansion functions are used, as in [5]. The additional term is $\sin k_o(y - H) + \alpha(1 - \cos k_o(y - H))$, where

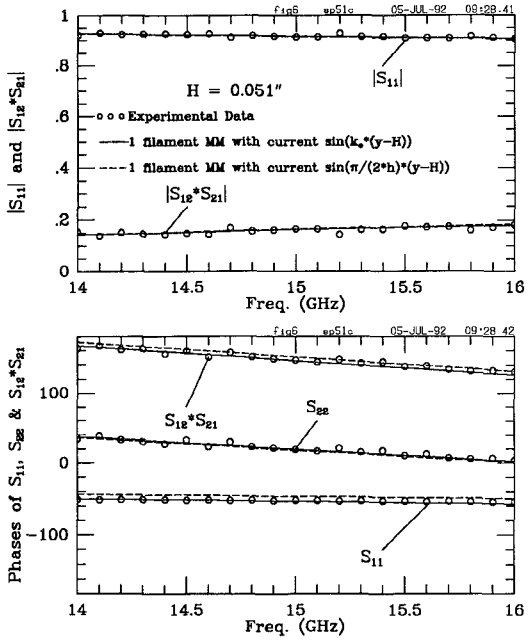

Fig 6. Scattering matrices of moment method's results and experimental data of a probe-excited cavity.

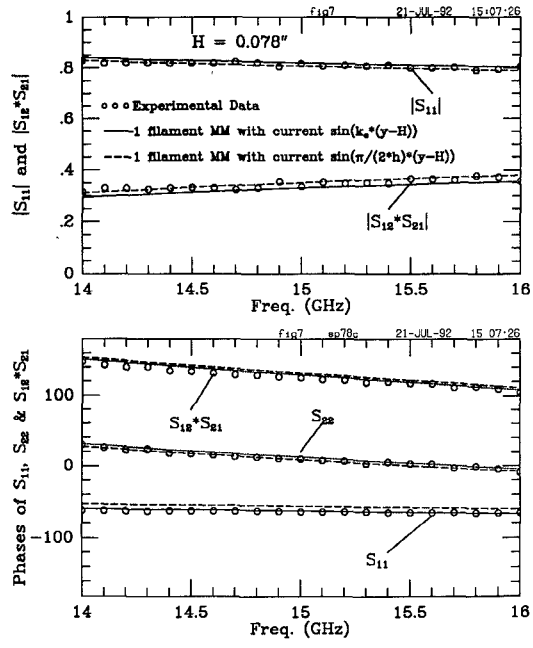

Fig. 7. Scattering matrices of moment method's results and experimental data of a probe-excited cavity.

α is constant to make this function orthogonal to $\sin k_o(y - H)$.

The frequency variation of the theoretical and experimental 2-port scattering matrices (both amplitude and phase) for two different probe's depths are shown in Fig. 6 and 7. Only one filament current is used but both the trial functions of (2) and (3) are computed. Experimental data agree well with the 3 cavities moment method solutions with either trial functions $\sin k_o(y - H)$ or $\sin \pi/2H(y - H)$ for loosely-coupled cases.

From the results and many computer simulations using each of the above described moment method computations, the following observations are noted:

1. The center-filament current approximation yields closer result to experiment than multifilament current modeling.
2. The three-cavity moment method yields better results than the direct semi-infinite waveguide but they are very close for very thin probe.
3. The computed phase of S_{22} is much closer to the experimental data than that of S_{11}.
4. For long probes, the numerical results are less accurate than for shorter probes.

The circuit parameters K and $\Delta\theta$ of the same probes as in Figs. 6 and 7 are shown in Fig. 8. The quantity $\Delta\theta$ in Fig. 8 is defined as the phase shift due to probe loading and is computed from

$$\Delta\theta = \pi - \frac{2(l_1 + l_2')}{\lambda_g}\pi \tag{20}$$

where l_2' is the location of shorted plane that makes the cavity resonate at the operating wavelength λ_g.

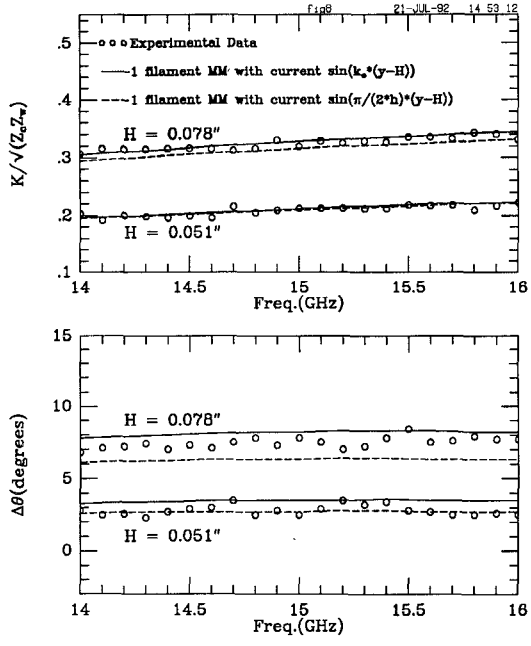

Fig. 8. Parameters K and $\Delta\theta$ of probe-excited cavities in Fig. 6 and 7.

Fig. 9 shows the variation of K, $\Delta\theta$ and external Q (Q_e) as a function of the probe depth.

Fig. 10(a) shows the dimensions of a probe-excited 6 pole, 0.05 dB ripple, 14.94 GHz, thick-iris filter. The design bandwidth is 420 MHz (2.8%) and the required input impedance inverter $K/\sqrt{Z_c Z_w}$ is 0.2679. The results of the input cavity design are listed in Table I and the sensitivities of the probe-excited cavity are listed in Table II.

Table III shows the amount of perturbation of each parameter for a residual reflection coefficient of 0.1 (i.e. maximum return loss of 13.7 dB), where ω_B is the relative bandwidth of the filter. It is observed that the residual

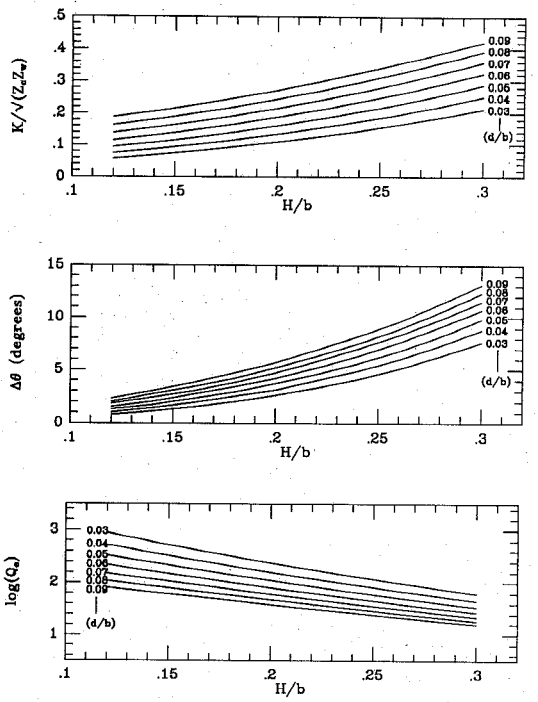

Fig. 9. K and $\Delta\theta$ and Q_e of probe-excited cavity.

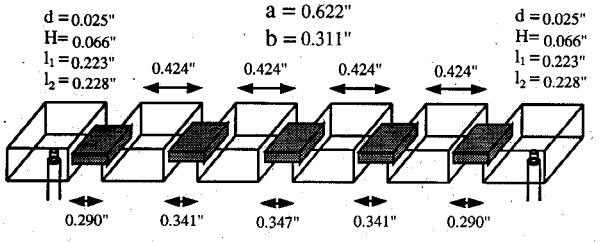

(a)

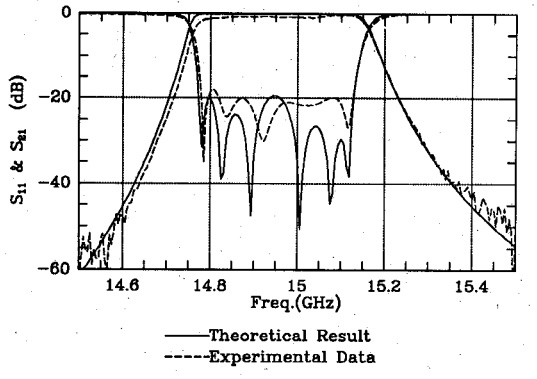

(b)

Fig. 10. (a) An experimental 6 poles, 0.05 dB ripple, thick iris filter. (b) Theoretical and experimental results of the filter in (a).

TABLE I
DESIGN VALUES OF THE PROBE-EXCITED INPUT/OUTPUT CAVITY OF THE FILTER IN FIG. 10(a)

l_1	l_2	H	K/Z_o	ϕ_2	$\Delta\theta$
0.223″	0.228″	0.066″	0.2679	85.2°	5.2°

TABLE II
COMPUTED SENSITIVITIES OF THE PROBE-EXCITED INPUT/OUTPUT CAVITY OF THE FILTER IN FIG. 10(a)

S_H^K	S_d^K	S_H^f	S_d^f	S_K^o
1.6%/mil	0.028/mil	0.098%/mil	0.075%/mil	0.95
S_f^o	S_H^o	S_d^o	$S_{\phi_2}^o$	$S_{\theta_2}^o$
12.2	0.028/mil	0.046/mil	0.075/per°	0.0375/per°

TABLE III
THE AMOUNT OF PERTURBATION THAT RESULTS IN 0.1 PASSBAND RESIDUAL REFLECTION COEFFICIENT OF THE FILTER IN FIG. 10(a) IN FIG. 10(a)

ΔH	Δd	$\Delta K/K$	$\Delta f/f$	$\Delta\phi_2$	$\Delta\theta_2$
3.75 mils	2.17 mils	10.5%	$0.29*\omega_B$	1.33°	2.66°

reflection coefficient due to perturbation of the resonant frequency and phase of S_{22} is roughly linearly dependent on the filter bandwidth for given order and passband ripple. This result indicates that the filter response is very sensitive to the phase of the return loss of the input/output coupling elements. For example, the value of $\Delta\theta_2$ in Table III is only about 1° for a 1% relative filter bandwidth.

Fig. 10(b) shows the computed and measured response of the filter in Fig. 10(a). The scattering matrices of the coupling irises are computed by the mode matching technique [2].

V. CONCLUSIONS

The three cavities moment method is used to numerically model probe-excited cavities. This method shows better agreement with experimental data than the semi-infinite waveguide method. The complete characterization of the coaxial to waveguide transition of a two port scattering matrix are obtained. Sensitivity analysis of the filter response to changes in the probe's dimensions and other filter design parameters are performed. Experimental measurements show excellent agreement with the numerical results of the probe-excited cavity. An experimental filter designed using the proposed probe model verified the validity of this model. The sensitivity analysis is a very powerful tool in determining the feasibility of the exact filter's design. This method is valuable for the design of high-dielectric-constant-filled miniature cavity filters.

APPENDIX

Let $G_{A_{yy}}(x, y, z; x', y', z')$ be the magnetic vector potential at field point (x, y, z) due to the unit y-directed electric current at source point (x', y', z') in a rectangular cavity as in Fig. 1(c). The $G_{F_{xx}}$ and $G_{F_{zz}}$ are the electrical vector potentials due to unit x- and z-directed magnetic current sources respectively. Follow the procedure in [3],

the following can be derived:

$$G_{A_{yy}}(x, y, z; x', y', z') = \sum_{n=1}^{\infty}\sum_{m=0}^{\infty} C_{mn} \sin k_x\left(x - \frac{a}{2}\right) \cos k_y y \sinh \gamma_{mn}(z + l_1), \quad \text{for } z \le z'$$
$$= \sum_{n=1}^{\infty}\sum_{m=0}^{\infty} D_{mn} \sin k_x\left(x - \frac{a}{2}\right) \cos k_y y \sinh \gamma_{mn}(z - l_2), \quad \text{for } z \ge z' \tag{A1}$$

where

$$C_{mn} = -\frac{4\mu}{ab\epsilon_{om}} \frac{\sin k_x(x' - a/2) \cos k_y y' \sinh \gamma_{mn}(z' - l_2)}{\gamma_{mn} \sinh \gamma_{mn}(l_1 + l_2)} \tag{A2}$$

$$D_{mn} = -\frac{4\mu}{ab\epsilon_{om}} \frac{\sin k_x(x' - a/2) \cos k_y y' \sinh \gamma_{mn}(z' + l_1)}{\gamma_{mn} \sinh \gamma_{mn}(l_1 + l_2)} \tag{A3}$$

$$G_{F_{xx}}(x, y, z; x', y', z') = \sum_{n=1}^{\infty}\sum_{m=0}^{\infty} A_{mn} \sin k_x\left(x - \frac{a}{2}\right) \cos k_y y \cosh \gamma_{mn}(z + l_1), \quad \text{for } z \le z'$$
$$= \sum_{n=1}^{\infty}\sum_{m=0}^{\infty} B_{mn} \sin k_x\left(x - \frac{a}{2}\right) \cos k_y y \cosh \gamma_{mn}(z - l_2), \quad \text{for } z \ge z' \tag{A4}$$

where

$$A_{mn} = -\frac{4\epsilon}{ab\epsilon_{om}} \frac{\sin k_x(x' - a/2) \cos k_y y' \cosh \gamma_{mn}(z' - l_2)}{\gamma_{mn} \sinh \gamma_{mn}(l_1 + l_2)} \tag{A5}$$

$$B_{mn} = -\frac{4\epsilon}{ab\epsilon_{om}} \frac{\sin k_x(x' - a/2) \cos k_y y' \cosh \gamma_{mn}(z' + l_1)}{\gamma_{mn} \sinh \gamma_{mn}(l_1 + l_2)} \tag{A6}$$

$$G_{F_{zz}}(x, y, z; x', y', z') = \sum_{n=1}^{\infty}\sum_{m=0}^{\infty} E_{mn} \cos k_x\left(x - \frac{a}{2}\right) \cos k_y y \sinh \gamma_{mn}(z + l_1), \quad \text{for } z \le z'$$
$$= \sum_{n=1}^{\infty}\sum_{m=0}^{\infty} F_{mn} \cos k_x\left(x - \frac{a}{2}\right) \cos k_y y \sinh \gamma_{mn}(z - l_2), \quad \text{for } z \ge z' \tag{A7}$$

where

$$E_{mn} = -\frac{4\epsilon}{ab\epsilon_{om}} \frac{\cos k_x(x' - a/2) \cos k_y y' \sinh \gamma_{mn}(z' - l_2)}{\gamma_{mn} \sinh \gamma_{mn}(l_1 + l_2)} \tag{A8}$$

$$F_{mn} = -\frac{4\epsilon}{ab\epsilon_{om}} \frac{\cos k_x(x' - a/2) \cos k_y y' \sinh \gamma_{mn}(z' + l_1)}{\gamma_{mn} \sinh \gamma_{mn}(l_1 + l_2)} \tag{A9}$$

where $k_x = n\pi/a$, $k_y = m\pi/b$ and $\gamma_{mn} = \sqrt{k_x^2 + k_y^2 - k_o^2}$, k_o is the free space wave number. ϵ_{om} is 2 for m equal 0 and is 1 otherwise.

For large m and n, γ_{mn} in (A1) approach $k_c = \sqrt{k_x^2 + k_y^2}$. Furthermore, if the condition $e^{-\gamma_{mn} l_i} \ll e^{-\gamma_{mn}|z - z'|}$, ($i$ = 1, 2) is true, the terms in (A1) that contain γ_{mn} approach the limit for large m, n:

$$\frac{\sinh \gamma_{mn}(z - l_2) \sinh \gamma_{mn}(z' + l_1)}{\gamma_{mn} \sinh \gamma_{mn}(l_1 + l_2)} \to \frac{-e^{k_c(|z - z'|)}}{2k_c} \tag{A10}$$

For $z \ge z'$, rearrange $G_{A_{yy}}$ as

$$G_{A_{yy}}(x, y, z; x', y', z') = -\frac{4\mu}{ab} \sum_{m=0}^{\infty} \frac{\cos k_y y' \cos k_y y}{\epsilon_{om}} \left\{ \sum_{n=1}^{\infty} \sin k_x(x' - a/2) \sin k_x(x - a/2) \right.$$
$$\cdot \left(\frac{\sinh \gamma_{mn}(z' + l_1) \sinh \gamma_{mn}(z - l_2)}{\gamma_{mn} \sinh \gamma_{mn}(l_1 + l_2)} + \frac{e^{-k_c|z - z'|}}{2k_c} \right) + \sum_{n=1}^{\infty} \sin k_x(x' - a/2)$$
$$\left. \cdot \sin k_x(x - a/2) \left(-\frac{e^{-k_c|z - z'|}}{2k_c} \right) \right\}. \tag{A11}$$

The second summation of index n, denoted as $S^{G_{A_{yy}}}_{m,\infty}$ can be rewritten as follows using Poisson's summation theory:

$$S^{G_{A_{yy}}}_{m,\infty} = \sum_{n=1}^{\infty} \sin k_x(x' - a/2) \sin k_x(x - a/2) \cdot \left(-\frac{e^{-k_c|z-z'|}}{2k_c}\right)$$

$$= -\frac{a}{4\pi} \operatorname{Re}\left\{\ln \frac{1 - e^{-j\pi/a(|x+x'+a|+j|z-z'|)}}{1 - e^{-j\pi/a(|x-x'|+j|z-z'|)}}\right\}, \quad m = 0$$

$$= -\frac{a}{4\pi} \sum_{n=-\infty}^{\infty} \cdot \{K_o(k_y\sqrt{(x - x' + 2na)^2 + (z - z')^2}) - K_o(k_y\sqrt{(x + x' + a + 2na)^2 + (z - z')^2})\}, \quad m \neq 0 \tag{A12}$$

where K_o is Bessel's function of 2nd kind. Using the following notations:

$$S^{G_{A_{yy}}}_{mn} = \frac{\sinh \gamma_{mn}(z' + l_1) \sinh \gamma_{mn}(z - l_2)}{\gamma_{mn} \sinh \gamma_{mn}(l_1 + l_2)} \tag{A13}$$

$$S^{G_{A_{yy}}}_{mn,\infty} = -\frac{e^{-k_c|z-z'|}}{2k_c} \tag{A14}$$

Equation (A1) can be rewritten as

$$G_{A_{yy}}(x, y, z; x', y', z') = -\frac{4\mu}{ab} \sum_{m=0}^{\infty} \frac{\cos k_y y' \cos k_y y}{\epsilon_{om}} \left\{\sum_{n=1}^{\infty} \sin k_x(x' - a/2) \cdot \sin k_x(x - a/2) (S^{G_{A_{yy}}}_{mn} - S^{G_{A_{yy}}}_{mn,\infty}) + S^{G_{A_{yy}}}_{m,\infty}\right\} \tag{A15}$$

Equation (A15) is used in numerical computation, since it converges faster than the original series.

Similarly, other Green's functions for the case of $z \geq z'$ can be transformed into fast convergent series using the same procedures as above. The results are listed below:

$$G_{F_{xx}}(x, y, z; x', y', z') = -\frac{4\mu}{ab} \sum_{m=0}^{\infty} \frac{\cos k_y y' \cos k_y y}{\epsilon_{om}} \left\{\sum_{n=1}^{\infty} \sin k_x(x' - a/2) \cdot \sin k_x(x - a/2) (S^{G_{F_{xx}}}_{mn} - S^{G_{F_{xx}}}_{mn,\infty}) + S^{G_{F_{xx}}}_{m,\infty}\right\} \tag{A16}$$

where

$$S^{G_{F_{xx}}}_{mn} = \frac{\cosh \gamma_{mn}(z' + l_1) \cosh \gamma_{mn}(z - l_2)}{\gamma_{mn} \sinh \gamma_{mn}(l_1 + l_2)} \tag{A17}$$

$$S^{G_{F_{xx}}}_{mn,\infty} = \frac{e^{-k_c|z-z'|}}{2k_c} \tag{A18}$$

$$S^{G_{F_{xx}}}_{m,\infty} = \sum_{n=1}^{\infty} \sin k_x(x' - a/2) \sin k_x(x - a/2) \cdot \left(\frac{e^{-k_c|z-z'|}}{2k_c}\right) = -S^{G_{A_{yy}}}_{m,\infty} \tag{A19}$$

$$G_{F_{zz}}(x, y, z; x', y', z') = -\frac{4\mu}{ab} \sum_{m=0}^{\infty} \frac{\cos k_y y' \cos k_y y}{\epsilon_{om}} \cdot \left\{\sum_{n=1}^{\infty} \cos k_x(x' - a/2) \cos k_x(x - a/2) \cdot (S^{G_{F_{zz}}}_{mn} - S^{G_{F_{zz}}}_{mn,\infty}) + S^{G_{F_{zz}}}_{m,\infty}\right\} \tag{A20}$$

where

$$S^{G_{F_{zz}}}_{mn} = \frac{\sinh \gamma_{mn}(z' + l_1) \sinh \gamma_{mn}(z - l_2)}{\gamma_{mn} \sinh \gamma_{mn}(l_1 + l_2)} \tag{A21}$$

$$S^{G_{F_{zz}}}_{mn,\infty} = \frac{e^{-k_c|z-z'|}}{2k_c} \tag{A22}$$

$$S^{G_{F_{zz}}}_{m,\infty} = \sum_{n=1}^{\infty} \cos k_x(x' - a/2) \cos k_x(x - a/2) \cdot \left(-\frac{e^{-k_c|z-z'|}}{2k_c}\right)$$

$$= -\frac{a}{4\pi} \operatorname{Re}\left\{\ln (1 - e^{-j\pi/a(|x+x'+a|+j|z-z'|)}\right\} + \ln (1 - e^{-j\pi/a(|x-x'|+j|z-z'|)}\Big\}, \quad m = 0$$

$$= -\frac{a}{4\pi} \sum_{n=-\infty}^{\infty} \cdot \{K_o(k_y\sqrt{(x - x' + 2na^2 + (z - z')^2})\}, \quad m = 0$$

$$+ K_o(k_y\sqrt{(x + x' + a + 2na)^2 + (z - z')^2})\} - \frac{1}{4k_y} e^{-k_y|z-z'|}, \quad m \neq 0 \tag{A23}$$

For the case of $z \leq z'$, just interchange z and z' in above equations.

References

[1] K. A. Zaki, C. Chen, and A. E. Atia, "A circuit model of probes in dual-mode cavities," *IEEE Trans. Microwave Theory Tech.*, vol. 36, pp. 1740–1745, Dec. 1988.

[2] H-C Chang and K. A. Zaki, "Evanescent-mode coupling of dual-mode rectangular waveguide filters," *IEEE Trans. Microwave Theory Tech.*, vol. 39, pp. 1307–1312, Aug. 1991.

[3] R. E. Collin, *Field Theory of Guided Waves*. New York: McGraw-Hill, 1960, pp. 258–271.

[4] A. G. Williamson and D. V. Otto, "Coaxial-fed hollow cylindrical monopole in a rectangular waveguide," *Electron. Lett.*, vol. 9, no. 10, pp. 218–220, May 17, 1973.
[5] J. M. Jarem, "A multifilament method-of moments solution for the input impedance of a probe-excited semi-infinite waveguide," *IEEE Trans. Microwave Theory Tech.*, vol. MTT-35, pp. 14–19, Jan. 1987.
[6] X. P. Liang and Kawthar A. Zaki, "Characterizing waveguide T-junctions by three plane mode-matching techniques," *1991 IEEE MTT-S Int. Microwave Symp. Dig.*, pp. 849–852.
[7] R. F. Harrington, *Time-Harmonic Electromagnetic Fields*. New York: McGraw-Hill, 1977, p. 127.
[8] Y. Leviatan, P. G. Li, A. T. Adams, and J. Perini, "Single-post inductive obstacle in rectangular waveguide," *IEEE Trans. Microwave Theory Tech.*, vol. MTT-15, pp. 806–811, Oct. 1983.
[9] R. F. Harrington, *Field Computation by Moment Method*. New York: Macmillan, 1968.
[10] W. L. Stutzman and G. A. Thiele, *Antenna Theory and Design*. New York: Wiley, 1981.
[11] H. P. Neff, Jr., C. A. Siller, Jr., and J. D. Tillman, Jr., "A simple approximation to the current on the surface of an isolated thin cylindrical center-fed dipole antenna of arbitrary length," *IEEE Trans. Antennas Propagat.*, vol. AP-18, pp. 399–400, May, 1970.
[12] G. Mathaei, L. Young, and E. M. T. Jones, *Microwave Filter, Impedance Matching Networks and Coupling Structures*. McGraw-Hill, New York, 1961, p. 432, p. 438.

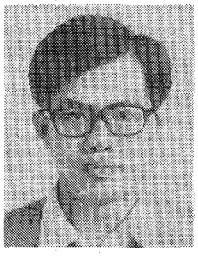

Ji-Fuh Liang was born in Taiwan, R.O.C., on Nov. 25, 1958. He received his B.S. degree in Electronics Engineering from National Chiao-Tung University, Taiwan in 1981, and M.S. degree in Electrical Engineering from National Taiwan University, Taiwan in 1985.

During the years 1981–1983, he was with the China military as a member of the technical staff. Beginning 1988, he spent three years as a member of technical staff and project leader at Microelectronics Technology Inc., Hsin-Chun Taiwan. Since 1989, he has been working as a research assistant in the Microwave Lab, Department of Electrical Engineering in UMCP. Currently, he is working toward his Ph.D. degree. His research interests include theoretical and experimental characterizations of microwave/milimeter-wave passive and active devices.

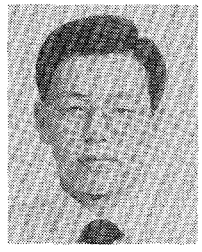

Hsin-Chin Chang was born in Taiwan, R.O.C., on June 13, 1963. He received his B.S. degree in Electrical Engineering from National Taiwan University in 1985, and M.S. degree in Electrical Engineering from University of Maryland, College Park in 1989.

Since 1987, he has been working as a research assistant in the Microwave Lab, Department of Electrical Engineering in UMCP. Currently, he is working toward his Ph.D. degree. His research interests include dielectric loaded waveguide characterizagions, dielectric loaded resonator filters, block filter designs, accurate waveguide filter characterizations and designs, MIC and MMIC designs, and numerical methods in Electromagnetism.

Kawthar A. Zaki (SM'85–F'91), for a photograph and biography, see this issue, p. 2302.